iScience

CellPress
OPEN ACCESS

Article

Partial prevention of glucocorticoid-induced osteocyte deterioration in young male mice with osteocrin gene therapy

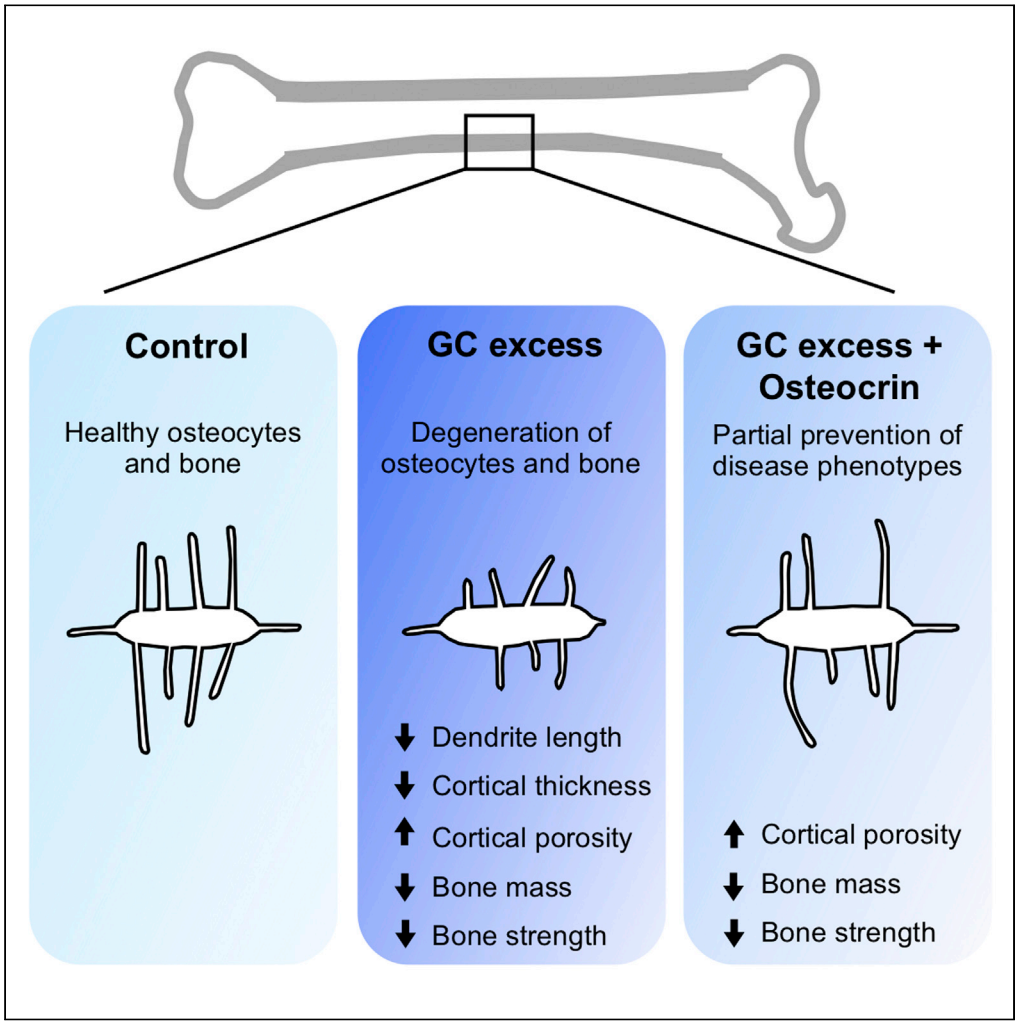

Courtney M. Mazur, Christian D. Castro Andrade, Nicha Tokavanich, ..., Mary L. Bouxsein, Jialiang S. Wang, Marc N. Wein

mnwein@mgh.harvard.edu

Highlights

Osteocyte degeneration is an early consequence of glucocorticoid (GC) excess

Osteocrin (Ostn) gene therapy protects osteocyte dendrites during GC excess in mice

Ostn preserves cortical thickness, but not bone mass or strength, during GC excess

Mazur et al., iScience 25, 105019
September 16, 2022
https://doi.org/10.1016/j.isci.2022.105019

iScience

CellPress
OPEN ACCESS

Article

Partial prevention of glucocorticoid-induced osteocyte deterioration in young male mice with osteocrin gene therapy

Courtney M. Mazur,[1] Christian D. Castro Andrade,[1] Nicha Tokavanich,[1] Tadatoshi Sato,[1] Michael Bruce,[1] Daniel J. Brooks,[1,2] Mary L. Bouxsein,[1,2] Jialiang S. Wang,[1] and Marc N. Wein[1,3,4,5,*]

SUMMARY

Glucocorticoid excess suppresses osteocyte remodeling of surrounding bone minerals, causes apoptosis of osteoblasts and osteocytes, and disrupts bone remodeling, eventually, leading to glucocorticoid-induced osteoporosis and bone fragility. Preventing apoptosis and preserving osteocyte morphology could be an effective means of preventing bone loss during glucocorticoid treatment. We hypothesized that osteocrin, which preserves osteocyte viability and morphology in Sp7-deficient mice, could prevent osteocyte death and dysfunction in a glucocorticoid excess model. We used adeno-associated virus (AAV8) to induce osteocrin overexpression in mice one week before implantation with prednisolone or placebo pellets. After 28 days, prednisolone caused the expected reduction in cortical bone thickness and osteocyte canalicular length in control AAV8-treated mice, and these effects were blunted in mice receiving AAV8-osteocrin. Glucocorticoid-induced changes in cortical porosity, trabecular bone mass, and gene expression were not prevented by osteocrin. These findings support a modest therapeutic potential for AAV8-osteocrin in preserving osteocyte morphology during disease.

INTRODUCTION

Long-term glucocorticoid (GC) treatment is a well-known cause of drug-induced osteoporosis and osteonecrosis. By reducing bone formation, increasing bone resorption, and reducing bone quality, glucocorticoids increase the risk of fragility fractures in a dose and duration-dependent manner (Buckley and Humphrey, 2018). Owing to the usefulness of glucocorticoids in treating patients with a wide variety of inflammatory conditions, many studies have investigated the effects of anti-resorptives and anabolic therapies for preserving bone mass during GC use. Bisphosphonates, denosumab, and teriparatide show some efficacy in improving bone mass and reducing fracture risk in patients receiving GCs (Reid et al., 2009; Saag et al., 2009, 2019; Stoch et al., 2009; Wallach et al., 2000). However, these treatments are accompanied by rare but serious side effects, such as increased risk of osteonecrosis, atypical fractures, and hypercalcemia (Khan et al., 2015; Khow et al., 2017; Saag et al., 2009), so improved therapies are needed. Furthermore, available therapies for GC-induced osteoporosis largely ignore osteocytes.

Healthy osteocytes play key roles in bone by secreting paracrine factors to coordinate the activity of osteoblasts and osteoclasts and by remodeling the bone matrix surrounding their lacuno-canalicular network. This local remodeling maintains the organization of the lacuno-canalicular network and contributes to bone material quality; genetic and pharmacological interventions that suppress osteocyte remodeling activity reduce bone quality and increase fragility (Alemi et al., 2018; Dole et al., 2017; Mazur et al., 2019). A large body of research demonstrates that high-dose glucocorticoid treatment induces osteocyte death in humans and in mice (Jia et al., 2011; Lane et al., 2006; O'Brien et al., 2004; Plotkin et al., 1999; Weinstein et al., 1998, 2000). Even before causing apoptosis, GC excess reduces the number and length of osteocyte dendritic projections and disrupts the ability of osteocytes to remodel the lacuno-canalicular network (Fowler et al., 2017; Lane et al., 2006; Plotkin et al., 2007). Preventing osteocyte apoptosis, preserving their dendritic phenotype, and maintaining remodeling activity during GC excess could be an effective method of combatting GC-induced osteoporosis and fragility.

[1]Endocrine Unit, Massachusetts General Hospital, Harvard Medical School, Boston, MA, USA

[2]Center for Advanced Orthopedic Studies, Department of Orthopedic Surgery, Beth Israel Deaconess Medical Center, Harvard Medical School, Boston, MA, USA

[3]Broad Institute of Harvard and MIT, Cambridge, MA, USA

[4]Harvard Stem Cell Institute, Cambridge, MA, USA

[5]Lead contact

*Correspondence: mnwein@mgh.harvard.edu

https://doi.org/10.1016/j.isci.2022.105019

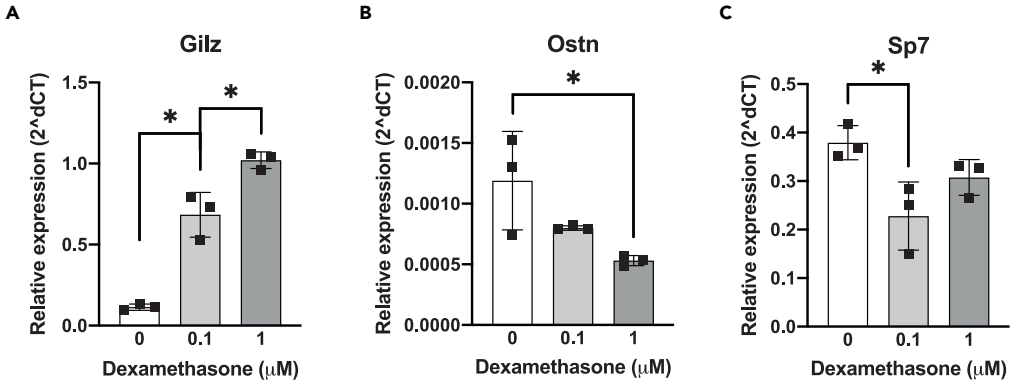

Figure 1. Glucocorticoids suppress *in vitro* Ostn expression

Ocy454 cells were treated with dexamethasone at the indicated concentrations for 3 h. Expression of (A) canonical glucocorticoid receptor target gene *Gilz*, (B) *Ostn*, and (C) transcription factor *Sp7* were measured by RT-qPCR and presented relative to *Actb*. n = 3. *p < 0.05 by Tukey's multiple comparisons tests. Error bars show +/− SD See also Figure S1.

We recently reported the role of the transcription factor Sp7 in osteocyte development (Wang et al., 2021). Conditional ablation of Sp7 causes reduced osteocyte dendrite number and length, apoptosis of embedded osteocytes, increased cortical porosity, and low bone mass in young mice. This phenotype can be rescued by overexpression of one of the genes whose levels are reduced by Sp7 deletion—osteocrin (Ostn). Ostn is a secreted peptide that occupies the natriuretic peptide receptor (NPR)-C, a clearance receptor, thereby preventing clearance of C-type natriuretic peptide (CNP). High levels of Ostn, therefore, increase CNP signaling through the guanylyl cyclase receptor NPR-B (Moffatt et al., 2007). downstream of NPR-B, CNP signaling leads to the production of cGMP, activation of protein kinase G, and action on a variety of targets including ERK phosphorylation and modulation of the cytoskeleton through RhoA and myosin light chain phosphatase (Hofmann et al., 2006). As Ostn overexpression was able to rescue osteocyte morphology and survival defects in Sp7 mutant mice, we hypothesized that overexpression of Ostn could prevent changes in osteocyte morphology and viability in response to GCs.

Here we tested the influence of systemically-administered Ostn via AAV8 gene therapy on the skeletal effects of GCs in mice. We report that AAV8-Ostn treatment blunted GC-induced effects such as reduction in cortical bone mass and osteocyte canalicular length. Despite these apparently-beneficial findings, we noted overall mild effects of GC treatment in this model and also observed that AAV8-Ostn therapy failed to rescue other skeletal consequences of GCs such as increased cortical bone porosity, reduced trabecular bone mass, and reduced flexural strength. Taken together, these data demonstrate potential beneficial effects of AAV8-Ostn therapy for osteocytes that may not fully combat this common cause of skeletal fragility.

RESULTS

Dexamethasone reduces osteocrin and integrin β3 expression *in vitro*

The goal of this study was to assess the therapeutic potential of osteocrin (Ostn) overexpression on GC-induced skeletal disease. To establish a rationale for this study, we started by testing the effects of GCs on Sp7 and Ostn expression in an osteocyte cell culture model. Dexamethasone treatment of Ocy454 cells, a conditionally-immortalized murine osteocyte-like cell line (Spatz et al., 2015), reduced both *Sp7* and *Ostn* mRNA expression in a dose-dependent manner while causing the expected increase in the canonical glucocorticoid receptor target gene *Gilz* (D'Adamio et al., 1997) (Figures 1A–1C).

Dexamethasone affects osteocyte cell projections before inducing apoptosis (Plotkin et al., 2007). We used the integrin β3 subunit, which forms dimers with the αV subunit along osteocyte dendritic projections, as a marker of healthy osteocyte dendrites in cells treated with glucocorticoids (Qin et al., 2020; Wang et al., 2007; Xie et al., 2018). After 24 h of dexamethasone treatment in Ocy454 cells, we found that integrin β3 mRNA (*Itgb3*) and surface expression (CD61 staining) were significantly reduced compared to vehicle-treated controls (Figures S1A and S1B). Pretreatment with CNP or Ostn + CNP attenuated dexamethasone-induced decreases in CD61 surface labeling (Figures S1C–S1E), indicating that the CNP signaling pathway can modulate the effects of glucocorticoids in osteocytes.

Kinetics of AAV8-mediated *Ostn* gene therapy

To determine the short-term kinetics of *Ostn* expression *in vivo* in response to the administration of the AAV8-Ostn vector, we conducted a pilot experiment in C57BL/6J mice. Importantly, AAV8 has a strong tropism for liver; therefore, this system delivers Ostn cDNA for hepatic expression with subsequent delivery of osteocrin protein to bone via the circulation (Nakai et al., 2005; Zincarelli et al., 2008). Mice were injected intraperitoneally with AAV8-Ostn and livers were collected 1, 3, or 7 days later. Expression of hepatic *Ostn* mRNA increased rapidly over the first three days of AAV8 infection and remained high at 7 days (Figure S2A). To allow for protein translation and transport to bone via circulation, a seven-day lead time was chosen for AAV8-Ostn injection before starting glucocorticoid treatment.

Effects of AAV8-Ostn on prednisolone-induced bone changes

One week after injection with AAV8-Ostn or AAV8-control vector, FVB mice—a strain reported to show robust glucocorticoid-induced bone loss (Fowler et al., 2017; Rauch et al., 2010; Thiele et al., 2012)—were implanted subcutaneously with continuous-release placebo or prednisolone pellets (2.8 mg/kg/d). Weekly monitoring of body weight showed that prednisolone-treated mice initially lost weight and maintained average body weights below those of placebo-treated mice (Figures S2C and S2D). Weight loss owing to muscle atrophy is a known consequence of high-dose glucocorticoid treatment in mice (Waddell et al., 2008), so these findings suggest the efficacy of the glucocorticoid excess model. Five weeks after AAV8 infection, hepatic *Ostn* expression remained elevated for mice implanted with both placebo and prednisolone pellets (Figure S2B), consistent with the documented persistence of AAV-mediated gene expression (Nakai et al., 2005; Zincarelli et al., 2008).

Similar to *in vitro* dexamethasone treatments, prednisolone reduced *Ostn* mRNA in marrow-depleted cortical bone collected from humeri of AAV8-control-treated mice (Figure 2A). At this time point, there was no detectable effect on *Sp7* mRNA in marrow-depleted bone tissue (Figure 2A). The suppression of *Ostn* by prednisolone *in vivo* further supports the rationale for our hypothesis that Ostn overexpression could rescue the deleterious skeletal effects of glucocorticoids. In contrast to previous mRNA analyses after 7 days of prednisolone treatment (Fowler et al., 2017), we did not find the induction of glucocorticoid-responsive *Gilz* or suppression of proteinase *Mmp13* in bone 28 days after prednisolone pellet implantation here. Osteocalcin (*Bglap*) is often suppressed in bone mRNA and in serum after glucocorticoid treatment (Piemontese et al., 2016; Thiele et al., 2012), but there was no significant effect of prednisolone on *Bglap* at this time point. We also did not observe differences in *Sost* or *Dkk1* mRNA in response to prednisolone (Figures S3A and S3B), though the regulation of these transcripts by glucocorticoids varies with treatment time and between studies (Thiele et al., 2012, 2019; Yao et al., 2008). However, we did detect significant induction of the osteoclast marker genes *Acp5* (encodes TRAP5b) and *Ctsk* (encodes Cathepsin K) by prednisolone in marrow-depleted bone tissue (Figure 2A). Prednisolone-induced increases in *Ctsk* and *Acp5* expression in bone were not prevented by AAV8-Ostn treatment (Figure 2B).

Ostn peptide enhances Erk1/2 phosphorylation in cultured osteoblasts and osteocytes (Wang et al., 2021), and here we show modest induction of the Erk1/2-responsive gene *Fos* (encodes cFos) by AAV8-Ostn treatment *in vivo* (Figure S4A). Bone *Fos* expression is significantly correlated with liver *Ostn* expression (Figure S4B), suggesting that the Ostn peptide encoded by AAV8-Ostn administration induces signaling and downstream gene expression changes in bone. Furthermore, consistent with our *in vitro* findings (Figures S1C–S1E), AAV8-Ostn significantly increased cortical bone *Itgb3* expression (Figure S4C).

In the femur, prednisolone caused the expected reduction in mid-diaphyseal cortical thickness in AAV8-control-treated mice (Fowler et al., 2017; Piemontese et al., 2016). In contrast, the effect of prednisolone on cortical thickness did not reach statistical significance in AAV8-Ostn-treated mice (Figures 3A and 3B). However, prednisolone significantly increased cortical porosity and decreased cortical area fraction in both AAV8-control and AAV8-Ostn-treated mice (Figure 3C and Table 1). Further supporting the efficacy of AAV8-Ostn treatment, comparison of all AAV8-control to all AAV8-Ostn-treated mice reveals a significant reduction in femoral cortical porosity with AAV8-Ostn (Figure 3C and Table 1, main effect of two-way ANOVA analysis), which is consistent with our previous studies in Sp7-deficient mice where AAV8-Ostn also reduced cortical porosity (Wang et al., 2021).

To assess the effect of glucocorticoids on cortical bone material properties, we measured flexural strength in the femur. As expected, prednisolone significantly reduced femoral bone structural and material

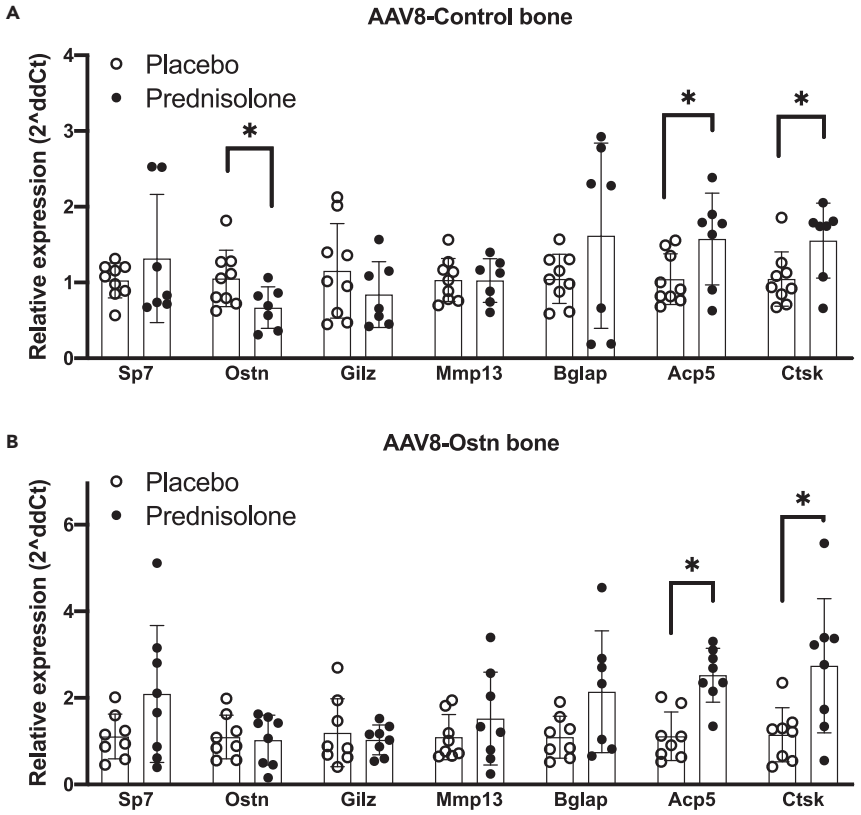

Figure 2. Prednisolone-induced changes in bone gene expression

Gene expression was measured relative to *Actb* in humeri after 28 days of prednisolone or placebo treatment in (A) AAV8-Control (n = 7-9) and (B) AAV8-Ostn-treated (n = 8) mice. *p < 0.05 compared to the corresponding placebo group by two-tailed t-tests. Error bars show +/− SD See also Figures S3 and S4.

properties including bending modulus, yield stress, and ultimate stress in both AAV8-control and AAV8-Ostn-treated mice (Figures 3D, 3E, and Table 2). Interestingly, AAV8-Ostn pretreatment exerted a slight protective effect on yield-related outcomes. Prednisolone reduced yield moment, yield stress, and work to yield by 26-38% in AAV8-control-treated mice and by 18-20% in AAV8-Ostn-treated mice (Figure 3F and Table 2). These changes in bone material properties further demonstrate deleterious skeletal effects of glucocorticoids in our study and suggest that Ostn may have a modest protective effect on bone material strength.

We also found that prednisolone reduced trabecular thickness, reduced trabecular bone mineral density (BMD), and increased trabecular structure model index (SMI) in the femur, but these effects were not mitigated by AAV8-Ostn (Figures 3G and 3H, Table 1). Prednisolone had minimal effect on trabecular bone in the axial skeleton (L5 vertebrae) as well, causing slight reductions in trabecular bone volume fraction (BV/TV) and BMD and an increase in SMI that was not mitigated by AAV8-Ostn (Table 3).

The relatively mild effects of prednisolone on trabecular bone mass are corroborated by its small effects on serum markers of bone turnover measured at study completion (4 weeks after prednisolone pellet implantation). Prednisolone did not cause significant changes in serum procollagen type 1 N-terminal peptide (P1NP) or C-terminal collagen crosslinks (CTX) in AAV8-control or AAV8-Ostn-treated mice (Figures 3I and 3J). Taken together, these micro-CT, flexural strength, and serum bone turnover marker data demonstrate mild changes in trabecular bone mass and bone remodeling in response to prednisolone administration in this study, with larger effects on cortical bone mass and strength. Mild, beneficial changes in cortical thickness and work to yield were noted in prednisolone-treated mice that also received AAV8-Ostn.

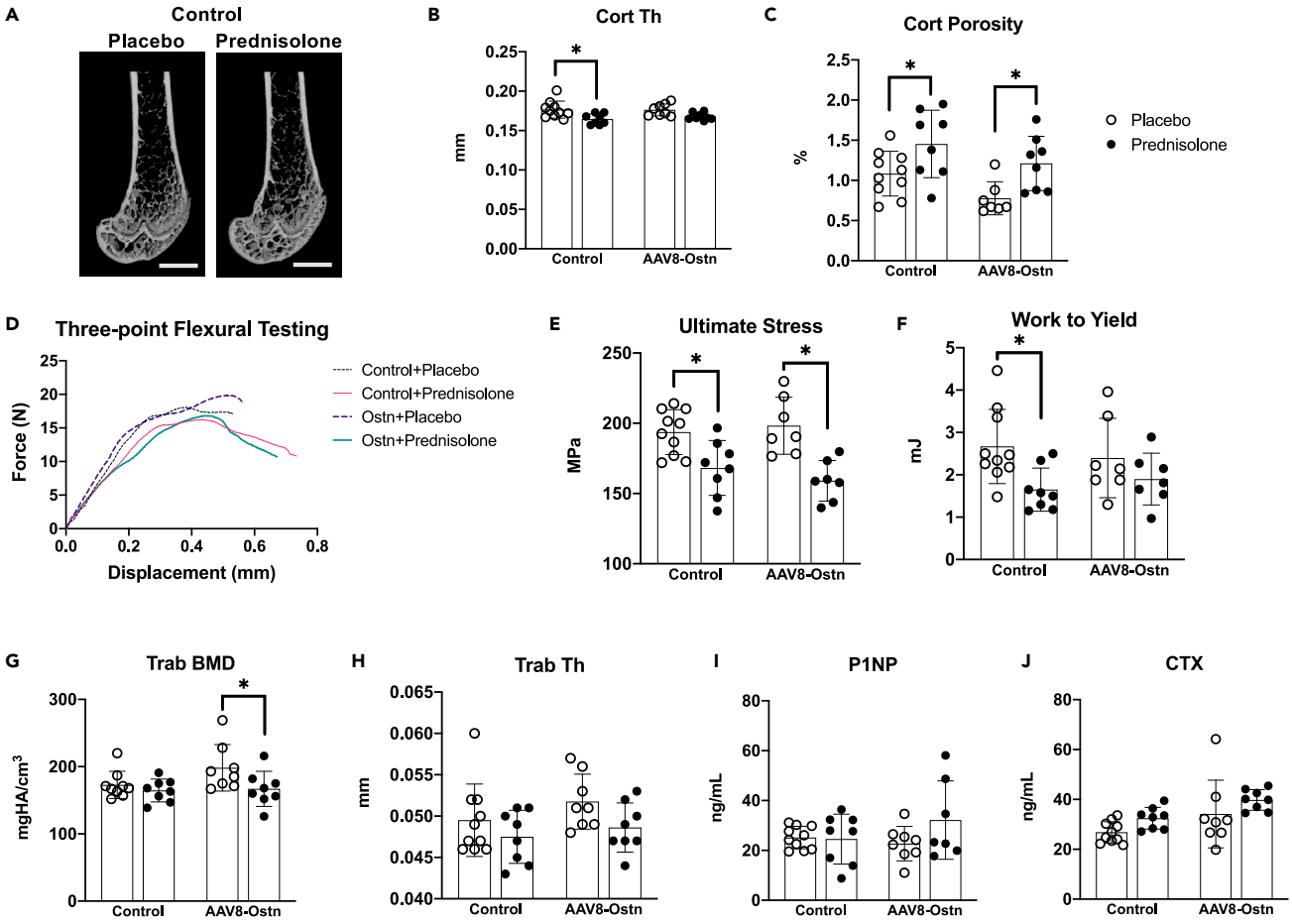

Figure 3. Prednisolone exerts a mild overall effect on bone mass, formation, and resorption

(A) Representative micro-CT images of the distal femur in AAV8-Control-treated mice after 28 days of placebo or prednisolone treatment. Scale bar = 1 mm.

(B) Cortical thickness (Cort Th) and (C) Cortical porosity (Cort porosity, one outlier removed from placebo + AAV8-Ostn group) were measured at the femoral mid-diaphysis.

(D) Representative force-displacement curves from three-point flexural testing of femurs.

(E) Ultimate stress and (F) work to yield were calculated from force-displacement curves from each sample and moment of inertia measured on the same bones.

(G) Trabecular bone mineral density (Trab BMD, one outlier removed from placebo + AAV8-Control group) and (H) Trabecular thickness (Trab Th) were measured in the distal femoral metaphysis.

(I) Serum biomarker of bone formation, procollagen type 1 N-terminal peptide (P1NP, one outlier removed from prednisolone + AAV8-Ostn group).

(J) Serum biomarker of bone formation, C-terminal collagen crosslinks (CTX). n = 7-10. *p < 0.05 compared to the corresponding placebo group by Sidak's multiple comparisons tests. All error bars show +/− SD.

Consistent with previous reports, we found strong osteocrin mRNA expression in the tibial periosteum via *in situ* hybridization (Figure 4A, top), predominantly on the antero-medial bone surface (Watanabe-Takano et al., 2021). As in our humerus RT-qPCR data, a modest reduction in periosteal Ostn expression was noted in AAV8-control + prednisolone-treated bones; fewer bones showed a strong mRNA signal and no Ostn mRNA was detected in one prednisolone-treated mouse (Figure 4A, bottom). This suggests that normal paracrine Ostn signaling from periosteal cells to osteocytes is disrupted during pharmacologic glucocorticoid excess.

Effects of prednisolone and AAV8-Ostn on osteocyte morphology and function

As endogenous expression of Ostn and the protective effects of AAV8-Ostn appeared to be limited to cortical bone, we conducted further histological analyses on cortical bone in the tibia. Consistent with RT-qPCR data in humeri, the number of TRAP-positive osteocytes was increased by prednisolone, though

Table 1. Microstructural properties of the femoral mid-diaphysis and metaphysis

	Placebo + Control (n = 10)	Placebo + AAV8-Ostn (n = 8)	Prednisolone + Control (n = 8)	Prednisolone + AAV8-Ostn (n = 8)
Bone length (mm)	14.56 ± 0.26	14.64 ± 0.46	14.35 ± 0.30	14.37 ± 0.57
BV/TV (%)	16.44 ± 2.67[a]	20.61 ± 5.38	15.56 ± 2.55	16.65 ± 3.80
BMD (mgHA/cm^3)	173 ± 20[a]	198 ± 35	164 ± 17[b]	167 ± 26[b,c]
Tb. N. (1/mm)	5.203 ± 0.514	5.479 ± 0.618	5.036 ± 0.575	5.119 ± 0.685
Tb. Th. (mm)	0.049 ± 0.004	0.052 ± 0.003	0.047 ± 0.003[b]	0.049 ± 0.003[b]
Tb. Sp. (mm)	0.192 ± 0.020	0.183 ± 0.021	0.200 ± 0.023	0.196 ± 0.030
SMI	1.951 ± 0.195[a]	1.621 ± 0.494	2.106 ± 0.253[b]	2.021 ± 0.335[b,c]
Ct. Th. (mm)	0.177 ± 0.011	0.176 ± 0.008	0.164 ± 0.007[b,c]	0.168 ± 0.005[b]
Ct. Ar./Tt. Ar. (%)	43.21 ± 1.64	42.90 ± 1.72	41.12 ± 1.80[b,c]	40.80 ± 1.22[b,c]
Ct. TMD (mgHA/cm^3)	1208 ± 8	1199 ± 13	1197 ± 12	1196 ± 6
Ct. Porosity (%)	1.08 ± 0.28	0.78 ± 0.21[d,a]	1.45 ± 0.42[b,c]	1.21 ± 0.34[d,b,c]

Properties measured in the femoral metaphysis include bone volume fraction (BV/TV), bone mineral density (BMD), trabecular number (Tb. N.), trabecular thickness (Tb. Th.), trabecular separation (Tb. Sp.) and structural model index (SMI). Properties measured at the femoral mid-diaphysis include cortical thickness (Ct. Th.), bone area fraction (Ct. At./Tt. Ar.), total mineral density (Ct. TMD), and cortical porosity (Ct. Porosity). All values are presented as mean ± SD

[a]One outlier removed.

[b]Overall effect of prednisolone $p < 0.05$, two-way ANOVA.

[c]$p < 0.05$ compared to the corresponding placebo group by Sidak's multiple comparisons tests.

[d]Overall effect of osteocrin $p < 0.05$, two-way ANOVA.

this difference only reached statistical significance in AAV8-Ostn mice (Figure 4B). Prednisolone did not significantly increase the frequency of empty osteocyte lacunae (Figure 4C) or the percentage of apoptotic (TUNEL-positive) osteocytes (Figure 4D), although TUNEL staining indicated trends toward increased apoptosis in response to both prednisolone and AAV8-Ostn. Although the effects of prednisolone on osteocyte TRAP expression and viability were mild, they were not prevented by AAV8-Ostn.

GC excess leads to early, deleterious changes in osteocyte morphology (Alemi et al., 2018; Fowler et al., 2017; Plotkin et al., 2007). To visualize the effects of prednisolone and AAV8-Ostn on the osteocyte canalicular network, we used both silver nitrate (stains extracellular matrix and cellular structures) and phalloidin staining (stains filamentous actin). In AAV8-control-treated mice, prednisolone significantly reduced canalicular length in silver nitrate-stained bone (Figure 5A) and density of phalloidin-stained cell projections (Figure 5B). Neither of these metrics was significantly altered by prednisolone in AAV8-Ostn-treated mice, and canalicular number was not affected in either group. These results indicate a modest protective effect of AAV8-Ostn on osteocyte morphology that does not correlate with detectable changes in osteocyte apoptosis at this timepoint.

DISCUSSION

This study tested the hypothesis that systemic treatment with liver-produced Ostn peptide could prevent harmful prednisolone-induced changes in bone strength, bone mass, osteocyte viability, and osteocyte morphology in cortical bone. After 4 weeks of prednisolone treatment, we found small changes in cortical thickness, canalicular length, and dendrite density that were significant only in control AAV8-treated mice. However, trabecular BMD and osteocyte TRAP staining were significantly changed by prednisolone in AAV8-Ostn treated mice, and cortical porosity, cortical area fraction, and bone strength were significantly changed by prednisolone irrespective of the AAV8 treatment group. Therefore, the apparent protective effects of Ostn on osteocyte morphology did not translate to functional improvements in osteocyte maintenance of bone. Although Ostn and other ligands of NPR-B/NPR-C may be useful at different doses or in different skeletal diseases, this study does not support a dramatic therapeutic benefit of Ostn to combat the deleterious skeletal effects of glucocorticoid excess.

Our hypothesis was supported by several studies showing the beneficial effects of Ostn and CNP in bone and growth plates of developing mice. High circulating Ostn in young mice stimulates bone growth in a

Table 2. Flexural properties of the femur. All values are presented as mean ± SD

	Placebo + Control (n = 10)	Placebo + AAV8-Ostn (n = 7)	Prednisolone + Control (n = 8)	Prednisolone + AAV8-Ostn (n = 7)
Bending Rigidity (N-mm^2)	751 ± 75	786 ± 66	608 ± 106[a,b]	613 ± 64[a,b]
Bending Modulus (GPa)	5.9 ± 0.7	5.9 ± 0.9	4.9 ± 0.9 [a,b]	4.6 ± 0.6[a,b]
Yield Moment (N-mm)	34.4 ± 5.7	33.8 ± 7.3	24.7 ± 4.4[a,b]	26.9 ± 5.4[a,b]
Yield Stress (MPa)	172.3 ± 19.3	160.5 ± 24	126.9 ± 23.5[a,b]	126.9 ± 22.6[a,b]
Ultimate Moment (N-mm)	38.7 ± 6.2	41.4 ± 4.8	32.7 ± 3.8[a,b]	33.7 ± 3.7[a,b]
Ultimate Stress (MPa)	193.7 ± 16.0	198.2 ± 20.3	168.2 ± 19.5[a,b]	162.3 ± 12.7[a,b]
Work to Yield (mJ)	2.67 ± 0.88	2.39 ± 0.93	1.65 ± 0.51[a,b]	1.96 ± 0.65[a]
Work to Fracture (mJ)	8.96 ± 3.7	8.73 ± 1.97	8.58 ± 2.71	8.57 ± 2.52
Post-yield Displacement (mm)	0.36 ± 0.19	0.35 ± 0.16	0.52 ± 0.24	0.51 ± 0.24

[a]Overall effect of prednisolone $p < 0.05$, two-way ANOVA.
[b]$p < 0.05$ compared to the corresponding placebo group by Sidak's multiple comparisons tests.

manner that depends on NPR-C and endogenous CNP expression (Kanai et al., 2017; Miyazaki et al., 2022). Likewise, enhancing CNP signaling through NPR-B regulates bone length, mineralization, and strength in growing mice (Robinson et al., 2020). Taken together, these findings led to the development and approval of the NPR-B agonist vosoritide for patients with achondroplasia (Savarirayan et al., 2019). Interestingly, rare human NPR-C mutations have been associated with high bone mass (Gregson et al., 2018). In mice lacking Sp7 expression in osteocytes, AAV8-Ostn treatment from 3 to 6 weeks old preserves osteocyte morphology, osteocyte viability, and cortical porosity (Wang et al., 2021). Recently, Watanabe-Takano et al. described that Ostn is involved in bone formation during recovery from unloading, suggesting an additional role for Ostn in mature bone (Watanabe-Takano et al., 2021).

Here we investigated whether mature osteocytes could also benefit from Ostn in a disease model. As in previous studies, this experiment used the liver to overexpress Ostn and deliver the peptide to bone (Kanai et al., 2017; Wang et al., 2021). We found that AAV8 infection of the liver caused rapid upregulation of *Ostn* mRNA that was still apparent at 35 days post-injection. To confirm that Ostn successfully targeted and induced signaling in bone, we measured the bone expression of *Fos*, which was proportional to hepatic *Ostn* expression. In contrast to the treatment of young developing mice (3-6 weeks old) lacking Sp7 in osteoblasts and osteocytes (Wang et al., 2021), osteocrin treatment here (7-12 weeks old) had few effects on osteocytes or bone. We observed that, as expected, AAV8-Ostn reduced cortical porosity. However, because AAV8-Ostn reduced osteocyte apoptosis and improved osteocyte morphology defects in Sp7 conditional knockout mice, we were surprised to see that Ostn tended to increase TUNEL staining in osteocytes here. The protective effect of osteocrin on canalicular length was somewhat more striking in the

Table 3. Microstructural properties of the fifth lumbar (L5) vertebral body

	Placebo + Control (n = 10)	Placebo + AAV8-Ostn (n = 7)	Prednisolone + Control (n = 7)	Prednisolone + AAV8-Ostn (n = 6)
BV/TV (%)	27.71 ± 2.73	29.71 ± 3.61	26.79 ± 2.47[a]	26.16 ± 2.80[a]
BMD (mgHA/cm^3)	275 ± 27	293 ± 31	266 ± 26[a]	260 ± 21[a]
Tb. N. (1/mm)	4.72 ± 0.31	4.73 ± 0.21	4.55 ± 0.22	4.74 ± 0.24
Tb. Th. (mm)	0.058 ± 0.003	0.061 ± 0.004	0.058 ± 0.005	0.056 ± 0.003
Tb. Sp. (mm)	0.211 ± 0.016	0.212 ± 0.011	0.220 ± 0.012	0.209 ± 0.010
ConnD. (1/mm^3)	194 ± 21	180 ± 18	193 ± 33	201 ± 22
SMI	0.317 ± 0.211	0.152 ± 0.343	0.447 ± 0.253[a]	0.542 ± 0.276[a,b]

Properties measured in the L5 vertebra include bone volume fraction (BV/TV), bone mineral density (BMD), trabecular number (Tb. N.), trabecular thickness (Tb. Th.), trabecular separation (Tb. Sp.), connectivity density (ConnD.) and structural model index (SMI). All values are presented as mean ± SD
[a]Overall effect of prednisolone $p < 0.05$, two-way ANOVA.
[b]$p < 0.05$ compared to the corresponding placebo group by Sidak's multiple comparisons tests.

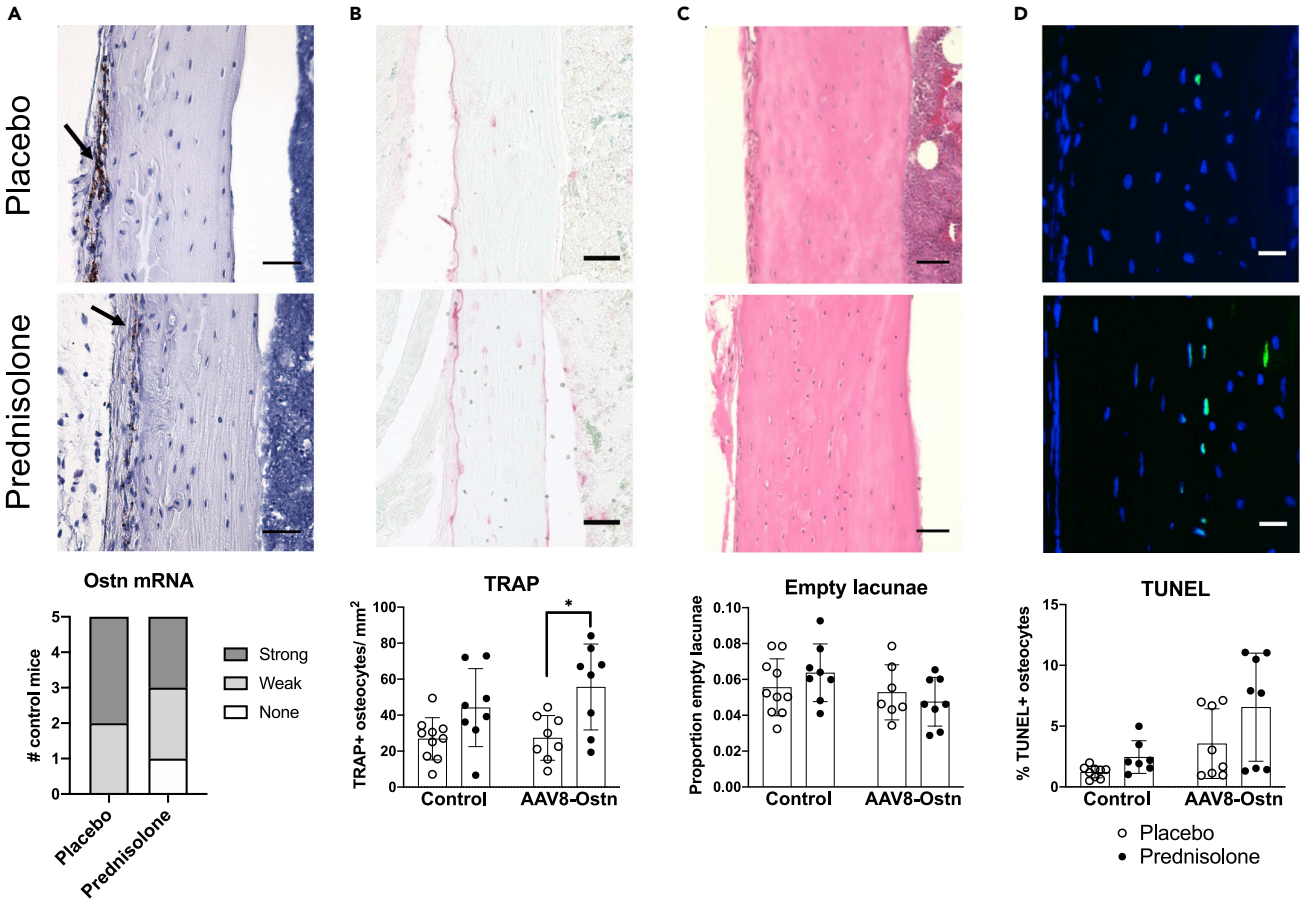

Figure 4. Prednisolone and AAV8-Ostn induce osteocyte apoptosis and TRAP expression in cortical bone

(A) Osteocrin mRNA expression was measured by *in situ* hybridization in AAV8-Control-treated cortical bone. Signal was semi-quantitatively analyzed but not statistically compared (n = 5). Arrows indicate signal in periosteum. Scale bar = 50 μm.

(B) Tartrate-resistant acid phosphatase (TRAP) expression was quantified as the number of positively stained osteocytes per cortical bone area. Images show AAV8-Control groups. Scale bar = 50 μm.

(C) Proportion of empty osteocyte lacunae was counted in hematoxylin and eosin-stained cortical bone. Images show AAV8-Control groups. Scale bar = 50 μm.

(D) Terminal deoxynucleotidyl transferase dUTP nick end labeling (TUNEL) was used to quantify apoptotic osteocytes in cortical bone (one outlier removed from placebo + AAV8-Control group and one outlier removed from prednisolone + AAV8-Control group). Scale bar = 20 μm. Images show AAV8-Control groups. n = 7-10. *p < 0.05 compared to the corresponding placebo group by Sidak's multiple comparisons tests. All error bars show +/− SD.

anterior tibia, so it is possible that osteocrin exerts site-specific effects related to cortical drift during development or proximity to endogenous osteocrin expression. These age and site-dependent differences will be important to consider as the mechanism and function of osteocrin are studied further.

Glucocorticoid-induced osteoporosis is a major cause of skeletal fragility and fractures. GCs effectively induce a "perfect storm" of changes in bone cells that culminates in increased bone resorption, reduced bone formation, and poor bone quality (Buckley and Humphrey, 2018). Defects in osteocyte activity and morphology and subsequent osteocyte apoptosis occur early in the course of GC therapy and likely play a central role in driving subsequent changes in remodeling on bone surfaces. Therefore, treatments that maintain or restore osteocyte morphology and viability represent a promising approach to meet this important unmet medical need. Here we showed that systemically-administered Ostn (via AAV8 gene therapy) could improve cortical thickness and osteocyte morphology, but other GC-induced changes were not rescued by AAV8-Ostn in this study. It remains possible that different molecular pathways lead to osteocyte dysfunction in the settings of Sp7 and GC treatment. Despite the limitations noted later in discussion, these findings demonstrate the therapeutic potential for AAV8-Ostn for common diseases caused by osteocyte

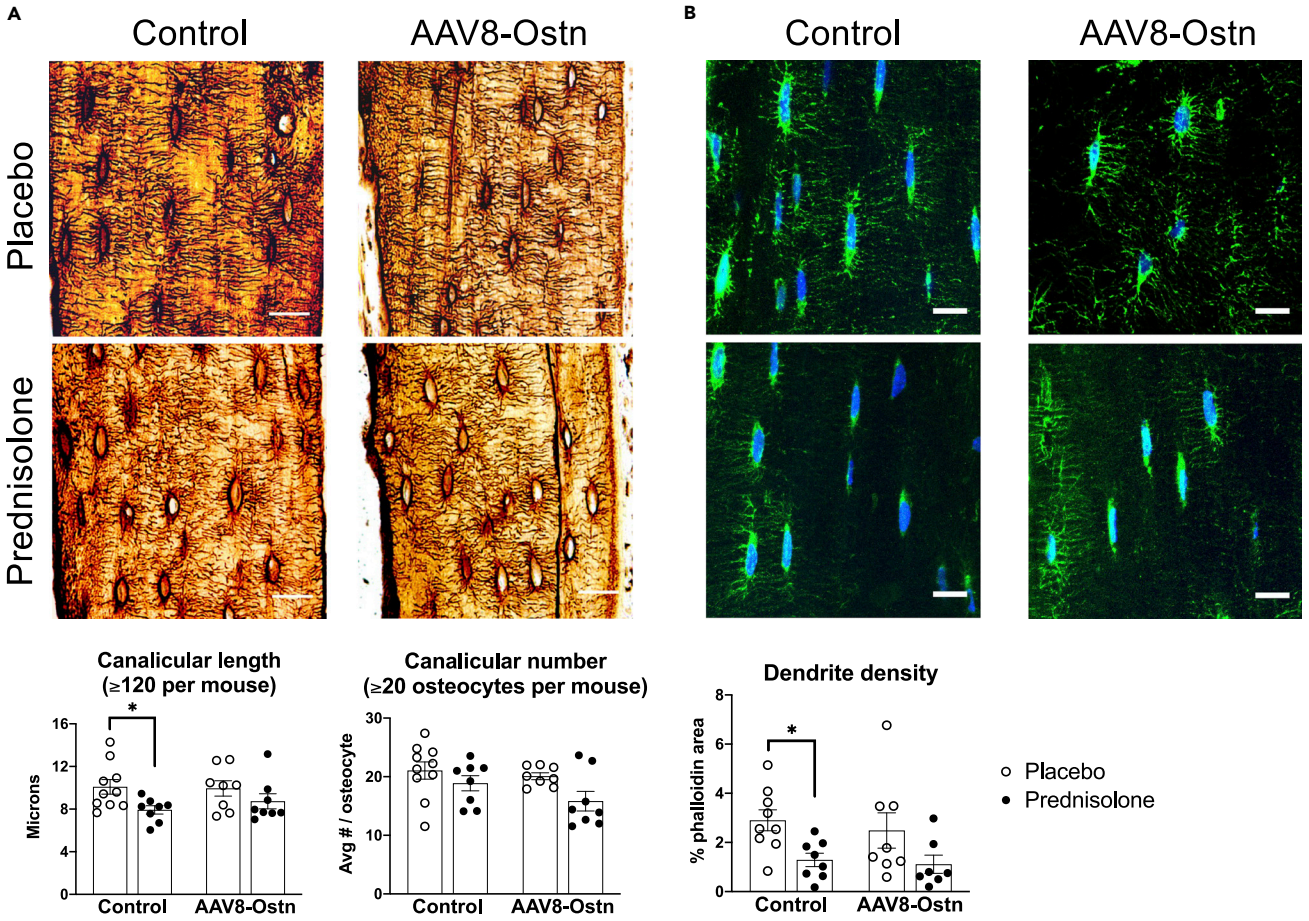

Figure 5. Prednisolone reduces the canalicular length and dendrite density in AAV8-Control mice only

(A) Canalicular length and canalicular number were measured in silver nitrate-stained cortical bone. Scale bar = 20 μm.

(B) Phalloidin staining of filamentousactin was used to measure the density of osteocyte dendrites (one outlier removed from placebo + AAV8-Control group and one outlier removed from prednisolone + AAV8-Ostn group). Scale bar = 10 μm n = 7-10. *p < 0.05 compared to the corresponding placebo group by Sidak's multiple comparisons tests. All error bars show +/− SEM.

dysfunction and support further study into the translational potential of different modalities of bone-directed Ostn therapy.

Limitations of the study

An important limitation of the current study is the mild overall effect of prednisolone on control mice. At similarly reported doses of prednisolone and 3-6 weeks of treatment, other studies have reported more robust changes in trabecular BV/TV, serum bone turnover markers, and osteocyte viability than were detected here (Ersek et al., 2016; Fowler et al., 2017; Jia et al., 2011; Lane et al., 2006; Shidara et al., 2019; Thiele et al., 2012; Weinstein et al., 1998). Changes in mouse body weight throughout the study period give us confidence in the efficacy of the glucocorticoid excess model, and we did find the expected prednisolone-induced changes in cortical thickness, cortical porosity, bone strength, and osteocyte morphology. Some of these outcomes may be time-dependent. For example, suppression of PLR genes was previously reported at 7 days and may be resolved or compensated for by 28 days (Fowler et al., 2017), and osteocyte viability would perhaps be more significantly different after a longer treatment period (Jia et al., 2011). Therefore, future time course studies may be needed to assess the effects of AAV8-Ostn on distinct prednisolone-induced skeletal changes. Furthermore, it is possible that the kinetics or pattern of AAV8-Ostn expression differs between the C57BL/6J mice used in pilot experiments and the FVB mice co-treated with prednisolone. We measured the robust liver expression of *Ostn* in AAV8-Ostn-treated FVB mice at the end of the experiment which was comparable in magnitude to that in C57BL/6J mice at

3-7 days post-injection, but a delay in Ostn peptide expression could have mitigated the efficacy of Ostn against prednisolone-induced skeletal changes. Finally, given the mild overall effect of prednisolone on our control mice, we cannot exclude the possibility that a higher dose/stronger overall effect of prednisolone would induce significant changes in mice treated with AAV8-Ostn. There were some apparent though statistically insignificant effects of prednisolone in AAV8-Ostn mice, and a larger effect in control mice or a larger sample size may tip the scales toward statistical significance in this group.

STAR★METHODS

Detailed methods are provided in the online version of this paper and include the following:

- KEY RESOURCES TABLE
- RESOURCE AVAILABILITY
  - Lead contact
  - Materials availability
  - Data and code availability
- EXPERIMENTAL MODEL AND SUBJECT DETAILS
  - Cell culture
  - Animals
- METHOD DETAILS
  - Serum
  - RNA
  - Micro-CT
  - Flexural testing
  - Histology
  - Image quantification
  - Flow cytometry
- QUANTIFICATION AND STATISTICAL ANALYSIS

SUPPLEMENTAL INFORMATION

Supplemental information can be found online at https://doi.org/10.1016/j.isci.2022.105019.

ACKNOWLEDGMENTS

We thank all members of the Wein laboratory for stimulating discussions. M.N.W. acknowledges funding support from the MGH Department of Medicine (Transformative Scholars award), the American Society for Bone and Mineral Research (Rising Star Award), and the National Institute of Health (AR067285). C.M.M. acknowledges support from the NIH (T32DK007028). M.N.W. and C.M.M. acknowledge generous support from Louise Pearl Corman, Ph.D. Micro-CT, flexural testing, and bone histology preparation were conducted by the Center for Skeletal Research, an NIH-funded program (P30 AR075042). Confocal microscopy was supported by the NIH Shared Instrumentation Grant (SIG) S10OD021577.

AUTHOR CONTRIBUTIONS

C.M.M., J.S.W., and M.N.W. conceived the study; C.M.M., C.D.C., T.S., M.B., and D.J.B. performed experiments; C.M.M., N.T., T.S., M.B., and D.J.B. analyzed the data; M.L.B. and M.N.W. supervised experiments and data analysis; C.M.M and M.N.W. wrote the article. All authors critically reviewed the article.

DECLARATION OF INTERESTS

M.N.W. acknowledges research support from Radius Health on unrelated projects. M.N.W. holds equity in and is a scientific advisory board member of Relation Therapeutics.

INCLUSION AND DIVERSITY STATEMENT

We worked to ensure diversity in experimental samples through the selection of the cell lines. One or more of the authors of this article self-identifies as an underrepresented ethnic minority in science. One or more of the authors of this article received support from a program designed to increase minority representation in science. Although citing references scientifically relevant for this work, we also actively worked to promote gender balance in our reference list. The author list of this article includes contributors from the

location where the research was conducted who participated in the data collection, design, analysis, and/or interpretation of the work.

Received: February 23, 2022
Revised: July 5, 2022
Accepted: August 19, 2022
Published: September 16, 2022

REFERENCES

Alemi, A.S., Mazur, C.M., Fowler, T.W., Woo, J.J., Knott, P.D., and Alliston, T. (2018). Glucocorticoids cause mandibular bone fragility and suppress osteocyte perilacunar-canalicular remodeling. Bone Rep. *9*, 145–153. https://doi.org/10.1016/j.bonr.2018.09.004.

Bouxsein, M.L., Boyd, S.K., Christiansen, B.A., Guldberg, R.E., Jepsen, K.J., and Müller, R. (2010). Guidelines for assessment of bone microstructure in rodents using micro–computed tomography. J. Bone Miner. Res. *25*, 1468–1486. https://doi.org/10.1002/JBMR.141.

Buckley, L., and Humphrey, M.B. (2018). Glucocorticoid-induced osteoporosis. N. Engl. J. Med. *379*, 2547–2556. https://doi.org/10.1056/NEJMCP1800214.

D'Adamio, F., Zollo, O., Moraca, R., Ayroldi, E., Bruscoli, S., Bartoli, A., Cannarile, L., Migliorati, G., and Riccardi, C. (1997). A new dexamethasone-induced gene of the leucine zipper family protects T lymphocytes from TCR/CD3-activated cell death. Immunity *7*, 803–812. https://doi.org/10.1016/S1074-7613(00)80398-2.

Dole, N.S., Mazur, C.M., Acevedo, C., Lopez, J.P., Monteiro, D.A., Fowler, T.W., Gludovatz, B., Walsh, F., Regan, J.N., Messina, S., et al. (2017). Osteocyte intrinsic TGFβ signaling regulates bone quality through perilacunar/canalicular remodeling. Cell Rep. *21*, 2585–2596. https://doi.org/10.1016/j.celrep.2017.10.115.

Ersek, A., Santo, A.I.E., Vattakuzhi, Y., George, S., Clark, A.R., and Horwood, N.J. (2016). Strain dependent differences in glucocorticoid-induced bone loss between C57BL/6J and CD-1 mice. Sci. Rep. *6*, 36513–36610. https://doi.org/10.1038/srep36513.

Fowler, T.W., Acevedo, C., Mazur, C.M., Hall-Glenn, F., Fields, A.J., Bale, H.A., Ritchie, R.O., Lotz, J.C., Vail, T.P., and Alliston, T. (2017). Glucocorticoid suppression of osteocyte perilacunar remodeling is associated with subchondral bone degeneration in osteonecrosis. Sci. Rep. *7*, 44618. https://doi.org/10.1038/srep44618.

Gregson, C.L., Newell, F., Leo, P.J., Clark, G.R., Paternoster, L., Marshall, M., Forgetta, V., Morris, J.A., Ge, B., Bao, X., et al. (2018). Genome-wide association study of extreme high bone mass: Contribution of common genetic variation to extreme BMD phenotypes and potential novel BMD-associated genes. Bone *114*, 62–71. https://doi.org/10.1016/j.bone.2018.06.001.

Hofmann, F., Feil, R., Kleppisch, T., and Schlossmann, J. (2006). Function of cGMP-dependent Protein Kinases as Revealed by Gene Deletion *86*, 1–23. https://doi.org/10.1152/PHYSREV.00015.2005.

Jia, J., Yao, W., Guan, M., Dai, W., Shahnazari, M., Kar, R., Bonewald, L., Jiang, J.X., and Lane, N.E. (2011). Glucocorticoid dose determines osteocyte cell fate. FASEB J. *25*, 3366–3376. https://doi.org/10.1096/fj.11-182519.

Kanai, Y., Yasoda, A., Mori, K.P., Watanabe-Takano, H., Nagai-Okatani, C., Yamashita, Y., Hirota, K., Ueda, Y., Yamauchi, I., Kondo, E., et al. (2017). Circulating osteocrin stimulates bone growth by limiting C-type natriuretic peptide clearance. J. Clin. Invest. *127*, 4136–4147. https://doi.org/10.1172/JCI94912.

Khan, A.A., Morrison, A., Hanley, D.A., Felsenberg, D., McCauley, L.K., O'Ryan, F., Reid, I.R., Ruggiero, S.L., Taguchi, A., Tetradis, S., et al.; International Task Force on Osteonecrosis of the Jaw (2015). Diagnosis and management of osteonecrosis of the jaw: a systematic review and international consensus. J. Bone Miner. Res. *30*, 3–23. https://doi.org/10.1002/JBMR.2405.

Khow, K.S.F., Shibu, P., Yu, S.C.Y., Chehade, M.J., and Visvanathan, R. (2017). Epidemiology and postoperative outcomes of atypical femoral fractures in older adults: a systematic review. J. Nutr. Health Aging *21*, 83–91. https://doi.org/10.1007/S12603-015-0652-3.

Lane, N.E., Yao, W., Balooch, M., Nalla, R.K., Balooch, G., Habelitz, S., Kinney, J.H., and Bonewald, L.F. (2006). Glucocorticoid-treated mice have localized changes in trabecular bone material properties and osteocyte lacunar size that are not observed in placebo-treated or estrogen-deficient mice. J. Bone Miner. Res. *21*, 466–476. https://doi.org/10.1359/JBMR.051103.

Mazur, C.M., Woo, J.J., Yee, C.S., Fields, A.J., Acevedo, C., Bailey, K.N., Kaya, S., Fowler, T.W., Lotz, J.C., Dang, A., et al. (2019). Osteocyte dysfunction promotes osteoarthritis through MMP13-dependent suppression of subchondral bone homeostasis. Bone Res. *7*, 34. https://doi.org/10.1038/s41413-019-0070-y.

Miyazaki, Y., Ichimura, A., Kitayama, R., Okamoto, N., Yasue, T., Liu, F., Kawabe, T., Nagatomo, H., Ueda, Y., Yamauchi, I., et al. (2022). C-type natriuretic peptide facilitates autonomic Ca(2+) entry in growth plate chondrocytes for stimulating bone growth. Elife *11*, e71931. https://doi.org/10.7554/eLife.71931.

Moffatt, P., Thomas, G., Sellin, K., Bessette, M.-C., Lafrenière, F., Akhouayri, O., St-Arnaud, R., and Lanctôt, C. (2007). Osteocrin is a specific ligand of the natriuretic peptide clearance receptor that modulates bone growth. J. Biol. Chem. *282*, 36454–36462. https://doi.org/10.1074/jbc.M708596200.

Nakai, H., Fuess, S., Storm, T.A., Muramatsu, S.i., Nara, Y., and Kay, M.A. (2005). Unrestricted hepatocyte transduction with adeno-associated virus serotype 8 vectors in mice. J. Virol. *79*, 214–224. https://doi.org/10.1128/jvi.79.1.214-224.2005.

O'Brien, C.A., Jia, D., Plotkin, L.I., Bellido, T., Powers, C.C., Stewart, S.A., Manolagas, S.C., and Weinstein, R.S. (2004). Glucocorticoids act directly on osteoblasts and osteocytes to induce their apoptosis and reduce bone formation and strength. Endocrinology *145*, 1835–1841. https://doi.org/10.1210/en.2003-0990.

Piemontese, M., Xiong, J., Fujiwara, Y., Thostenson, J.D., and O'Brien, C.A. (2016). Cortical bone loss caused by glucocorticoid excess requires RANKL production by osteocytes and is associated with reduced OPG expression in mice. Am. J. Physiol. Endocrinol. Metab. *311*, E587–E593. https://doi.org/10.1152/AJPENDO.00219.2016.

Plotkin, L.I., Weinstein, R.S., Parfitt, A.M., Roberson, P.K., Manolagas, S.C., and Bellido, T. (1999). Prevention of osteocyte and osteoblast apoptosis by bisphosphonates and calcitonin. J. Clin. Invest. *104*, 1363–1374. https://doi.org/10.1172/JCI6800.

Plotkin, L.I., Manolagas, S.C., and Bellido, T. (2007). Glucocorticoids induce osteocyte apoptosis by blocking Focal adhesion kinase-mediated survival. J. Biol. Chem. *282*, 24120–24130. https://doi.org/10.1074/JBC.M611435200.

Qin, L., Liu, W., Cao, H., and Xiao, G. (2020). Molecular mechanosensors in osteocytes. Bone Res. *8*, 23. https://doi.org/10.1038/s41413-020-0099-y.

Rauch, A., Seitz, S., Baschant, U., Schilling, A.F., Illing, A., Stride, B., Kirilov, M., Mandic, V., Takacz, A., Schmidt-Ullrich, R., et al. (2010). Glucocorticoids suppress bone formation by attenuating osteoblast differentiation via the monomeric glucocorticoid receptor. Cell Metab. *11*, 517–531. https://doi.org/10.1016/J.CMET.2010.05.005.

Reid, D.M., Devogelaer, J.P., Saag, K., Roux, C., Lau, C.S., Reginster, J.Y., Papanastasiou, P., Ferreira, A., Hartl, F., Fashola, T., et al.; HORIZON investigators (2009). Zoledronic acid and risedronate in the prevention and treatment of glucocorticoid-induced osteoporosis (HORIZON): a multicentre, double-blind, double-dummy, randomised controlled trial. Lancet *373*, 1253–1263. https://doi.org/10.1016/S0140-6736(09)60250-6.

Robinson, J.W., Blixt, N.C., Norton, A., Mansky, K.C., Ye, Z., Aparicio, C., Wagner, B.M., Benton, A.M., Warren, G.L., Khosla, S., et al. (2020). Male mice with elevated C-type natriuretic

peptide-dependent guanylyl cyclase-B activity have increased osteoblasts, bone mass and bone strength. Bone *135*, 115320. https://doi.org/10.1016/j.bone.2020.115320.

Saag, K.G., Pannacciulli, N., Geusens, P., Adachi, J.D., Messina, O.D., Morales-Torres, J., Emkey, R., Butler, P.W., Yin, X., and Lems, W.F. (2019). Denosumab versus risedronate in glucocorticoid-induced osteoporosis: final results of a twenty-four–month randomized, double-blind, double-dummy trial. Arthritis Rheumatol. *71*, 1174–1184. https://doi.org/10.1002/ART.40874.

Saag, K.G., Zanchetta, J.R., Devogelaer, J.P., Adler, R.A., Eastell, R., See, K., Krege, J.H., Krohn, K., and Warner, M.R. (2009). Effects of teriparatide versus alendronate for treating glucocorticoid-induced osteoporosis: thirty-six-month results of a randomized, double-blind, controlled trial. Arthritis Rheum. *60*, 3346–3355. https://doi.org/10.1002/ART.24879.

Sato, T., Verma, S., Andrade, C.D.C., Omeara, M., Campbell, N., Wang, J.S., Cetinbas, M., Lang, A., Ausk, B.J., Brooks, D.J., et al. (2020). A FAK/HDAC5 signaling axis controls osteocyte mechanotransduction. Nat. Commun. *11*, 3282–3318. https://doi.org/10.1038/s41467-020-17099-3.

Savarirayan, R., Irving, M., Bacino, C.A., Bostwick, B., Charrow, J., Cormier-Daire, V., Le Quan Sang, K.-H., Dickson, P., Harmatz, P., Phillips, J., et al. (2019). C-type natriuretic peptide analogue therapy in Children with achondroplasia. N. Engl. J. Med. *381*, 25–35. https://doi.org/10.1056/NEJMoa1813446.

Shidara, K., Mohan, G., Evan Lay, Y.A., Jepsen, K.J., Yao, W., and Lane, N.E. (2019). Strain-specific differences in the development of bone loss and incidence of osteonecrosis following glucocorticoid treatment in two different mouse strains. J. Orthop. Translat. *16*, 91–101. https://doi.org/10.1016/J.JOT.2018.07.001.

Spatz, J.M., Wein, M.N., Gooi, J.H., Qu, Y., Garr, J.L., Liu, S., Barry, K.J., Uda, Y., Lai, F., Dedic, C., et al. (2015). The wnt inhibitor sclerostin is up-regulated by mechanical unloading in osteocytes in vitro. J. Biol. Chem. *290*, 16744–16758. https://doi.org/10.1074/jbc.M114.628313.

Stoch, S.A., Saag, K.G., Greenwald, M., Sebba, A.I., Cohen, S., Verbruggen, N., Giezek, H., West, J., and Schnitzer, T.J. (2009). Once-weekly oral alendronate 70 mg in patients with glucocorticoid-induced bone loss: a 12-month randomized, placebo-controlled clinical trial. J. Rheumatol. *36*, 1705–1714. https://doi.org/10.3899/JRHEUM.081207.

Thiele, S., Hannemann, A., Winzer, M., Baschant, U., Weidner, H., Nauck, M., Thakker, R.V., Bornhäuser, M., Hofbauer, L.C., and Rauner, M. (2019). Regulation of sclerostin in glucocorticoid-induced osteoporosis (GIO) in mice and humans. Endocr. Connect. *8*, 923–934. https://doi.org/10.1530/EC-19-0104.

Thiele, S., Ziegler, N., Tsourdi, E., De Bosscher, K., Tuckermann, J.P., Hofbauer, L.C., and Rauner, M. (2012). Selective glucocorticoid receptor modulation maintains bone mineral density in mice. J. Bone Miner. Res. *27*, 2242–2250. https://doi.org/10.1002/JBMR.1688.

Waddell, D.S., Baehr, L.M., van den Brandt, J., Johnsen, S.A., Reichardt, H.M., Furlow, J.D., and Bodine, S.C. (2008). The glucocorticoid receptor and FOXO1 synergistically activate the skeletal muscle atrophy-associated MuRF1 gene. Am. J. Physiol. Endocrinol. Metab. *295*, 785–797. https://doi.org/10.1152/AJPENDO.00646.2007.

Wallach, S., Cohen, S., Reid, D.M., Hughes, R.A., Hosking, D.J., Laan, R.F., Doherty, S.M., Maricic, M., Rosen, C., Brown, J., et al. (2000). Effects of risedronate treatment on bone density and vertebral fracture in patients on corticosteroid therapy. Calcif. Tissue Int. *67*, 277–285. https://doi.org/10.1007/S002230001146.

Wang, J.S., Kamath, T., Mazur, C.M., Mirzamohammadi, F., Rotter, D., Hojo, H., Castro, C.D., Tokavanich, N., Patel, R., Govea, N., et al. (2021). Control of osteocyte dendrite formation by Sp7 and its target gene osteocrin. Nat. Commun. *12*, 6271–6320. https://doi.org/10.1038/s41467-021-26571-7.

Wang, Y., McNamara, L.M., Schaffler, M.B., and Weinbaum, S. (2007). A model for the role of integrins in flow induced mechanotransduction in osteocytes. Proc. Natl. Acad. Sci. USA *104*, 15941–15946. https://doi.org/10.1073/pnas.0707246104.

Watanabe-Takano, H., Ochi, H., Chiba, A., Matsuo, A., Kanai, Y., Fukuhara, S., Ito, N., Sako, K., Miyazaki, T., Tainaka, K., et al. (2021). Mechanical load regulates bone growth via periosteal Osteocrin. Cell Rep. *36*, 109380. https://doi.org/10.1016/j.celrep.2021.109380.

Wein, M.N., Liang, Y., Goransson, O., Sundberg, T.B., Wang, J., Williams, E.A., O, M.J., Govea, N., Beqo, B., Nishimori, S., et al. (2016). SIKs control osteocyte responses to parathyroid hormone. Nat. Commun. *7*. https://doi.org/10.1038/ncomms13176.

Weinstein, R.S., Jilka, R.L., Parfitt, A.M., and Manolagas, S.C. (1998). Inhibition of osteoblastogenesis and promotion of apoptosis of osteoblasts and osteocytes by glucocorticoids. Potential mechanisms of their deleterious effects on bone. J. Clin. Invest. *102*, 274–282. https://doi.org/10.1172/JCI2799.

Weinstein, R.S., Nicholas, R.W., and Manolagas, S.C. (2000). Apoptosis of osteocytes in glucocorticoid-induced osteonecrosis of the hip. J. Clin. Endocrinol. Metab. *85*, 2907–2912. https://doi.org/10.1210/jcem.85.8.6714.

Xie, J., Zhou, C., Zhang, D., Cai, L., Du, W., Li, X., and Zhou, X. (2018). Compliant substratum changes osteocyte functions: the role of ITGB3/FAK/β-Catenin signaling matters. ACS Appl. Bio Mater. *1*, 792–801. https://doi.org/10.1021/acsabm.8b00246.

Yao, W., Cheng, Z., Busse, C., Pham, A., Nakamura, M.C., and Lane, N.E. (2008). Glucocorticoid excess in mice results in early activation of osteoclastogenesis and adipogenesis and prolonged suppression of osteogenesis: a longitudinal study of gene expression in bone tissue from glucocorticoid-treated mice. Arthritis Rheum. *58*, 1674–1686. https://doi.org/10.1002/ART.23454.

Zincarelli, C., Soltys, S., Rengo, G., and Rabinowitz, J.E. (2008). Analysis of AAV serotypes 1-9 mediated gene expression and tropism in mice after systemic injection. Mol. Ther. *16*, 1073–1080. https://doi.org/10.1038/MT.2008.76.

STAR★METHODS

KEY RESOURCES TABLE

REAGENT or RESOURCE	SOURCE	IDENTIFIER
Antibodies		
Armenian Hamster anti-cd61, PE	Invitrogen	Cat#12-0611-82
Armenian Hamster IgG, PE	Invitrogen	Cat#12-4888-81
Bacterial and virus strains		
AAV8-CAG-mOstn-WPRE	Vector Biolabs	NA
AAV8-CAG-eGFP	Vector Biolabs	NA
Chemicals, peptides, and recombinant proteins		
Dexamethasone	Sigma	Cat#D2915
Annexin V, Alexa Fluor 488 conjugate	Invitrogen	Cat#A13201
Annexin Binding Buffer, 5x	Invitrogen	Cat#V13246
C-type natriuretic peptide (CNP)	Sigma	Cat#N8768
Osteocrin (Ostn) (83-132) peptide	Phoenix Pharmaceuticals	Cat#028-66
Prednisolone pellets	Innovative Research of America	Cat#SG-151
Placebo pellets	Innovative Research of America	Cat#SC-111
Buprenorphine HCl	Par Pharmaceutical	NDC 42023-179-05
Silver nitrate	Sigma	Cat#10220
Gelatin type A	Sigma	Cat#G2500
Formic acid	Millipore Sigma	Cat#FX0440
Sodium thiosulfate	Sigma	Cat#72049
Napthol AS-MX Phosphate	Sigma	Cat#N4875
Fast Red TR salt	Sigma	Cat#F6760
Fluoromount-G	SouthernBiotech	Cat#0100-01
TRIzol Reagent	Invitrogen	Cat#15596026
DAPI	Invitrogen	Cat#D1306
Proteinase K	Thermo Fisher	Cat#EO0492
Pepsin	Sigma	Cat#R2283
Critical commercial assays		
P1NP EIA	IDS	Cat#AC-33F1
CTX-1 EIA	IDS	Cat#AC-06F1
In Situ Cell Death Detection kit, fluorescein (TUNEL)	Roche	Cat#11684795910
CytoPainter F-actin staining kit - Green	Abcam	Cat#ab112125
PureLink RNA Mini Kit	Invitrogen	Cat#12183025
PerfeCT SYBR Green FastMix	Quantabio	Cat#95073
PrimeScript RT Reagent Kit with gDNA Eraser	Takara	Cat#RR047B
Experimental models: Cell lines		
Ocy454	PMID: 25271055	NA
Experimental models: Organisms/strains		
C57BL/6J Mice	The Jackson Laboratory	000,664
FVB Mice	The Jackson Laboratory	001,800

(*Continued on next page*)

Continued

REAGENT or RESOURCE	SOURCE	IDENTIFIER
Oligonucleotides		
RNAscope probe: Ostn	ACD	Cat#440791
Full list of qRT-PCR primers, see Table S1	This paper	NA
Software and algorithms		
Prism v8.4	GraphPad	https://www.graphpad.com/scientific-software/prism/
ImageJ	PMID: 22,930,834	https://imagej.nih.gov/ij/
FlowJo v10.7	BD	https://www.flowjo.com/
Other		
Trochar	Innovative Research of America	Cat#MP-182
Vetbond tissue adhesive	3M	Cat#1469SB
Serum separator tubes	BD	Cat#365967

RESOURCE AVAILABILITY

Lead contact

Requests for further information, resources, and reagents should be directed to and will be fulfilled by the Lead Contact, Marc Wein (mnwein@mgh.harvard.edu).

Materials availability

This study did not generate new unique reagents.

Data and code availability

- Raw data reported in this paper will be shared by the lead contact upon request.
- This work did not generate original code.
- Any additional information required to reanalyze the data reported in this paper is available from the lead contact upon request.

EXPERIMENTAL MODEL AND SUBJECT DETAILS

Cell culture

Ocy454 cells are osteocyte-like cells originally harvested from female mice (Spatz et al., 2015). Cells were maintained in alpha-minimum essential medium (MEM) supplemented with heat-inactivated 10% fetal bovine serum and 1% antibiotic–antimycotic (Gibco) at 33°C with 5% CO_2. Cells were transferred to 37°C to inactivate the temperature-sensitive T antigen and promote osteocytic differentiation. They were routinely assessed by *Sost* and *Dmp1* expression at 37°C as previously described (Sato et al., 2020; Wein et al., 2016).

For gene expression analysis, Ocy454 cells were grown in 24-well plates at 33°C until confluent, then differentiated at 37°C for 7 days. Dexamethasone (Sigma) was prepared in water and added to culture media at the indicated final concentrations, with water vehicle added to control groups at equal volume. After 3 h of treatment cells were washed and lysed in RLT. Lysate was passed through QIAshredder columns (Qiagen), then RNA was purified with PureLink columns (Invitrogen) and reverse transcribed to cDNA as described below.

For analysis of integrin β3 (cd61) surface expression, Ocy454 cells were grown in 24-well plates at 33°C until confluent, then differentiated at 37°C for 6 days. Cells were pretreated with CNP (100 nM), CNP + Ostn (100 nM + 500 nM), or vehicle (H2O) for 1 h, and then dexamethasone (1 μM) or vehicle was added for 24 h. On differentiation day 7, cells were dissociated in 0.05% trypsin-EDTA, collected and washed in FACS buffer (2% FBS in PBS), and then prepared for flow cytometry as described below. Each experiment was performed at least three times with three biologic replicates per condition in each experiment.

Animals

6-week-old male C57BL/6J and 6-week-old male FVB mice were purchased from Jackson Labs. For pilot experiments in C57BL/6J mice, 12 animals were randomized into four weight-matched groups at 7 weeks old and injected intraperitoneally with AAV8-CAG-eGFP in 100 uL saline ($5*10^{11}$ genome copies/mouse, Vector Biolabs). Mice were euthanized at 24 h, 3 days, and 7 days-post-injection for quantification of *Ostn* expression in liver.

35 FVB mice were randomized into four weight-matched groups at 7 weeks old and injected intraperitoneally with either AAV8-CAG-mOstn-WPRE or AAV8-CAG-eGFP in 100 uL saline ($5*10^{11}$ genome copies/mouse, Vector Biolabs). At 8 weeks old, FVB mice treated with each AAV were then implanted with slow-release prednisolone or placebo pellets giving an average dose of 2.8 mg/kg/day (4.3 mg; 60-day release; Innovative Research of America). Before the procedure, mice were anesthetized with isofluorane and given one dose of long-acting buprenorphine (0.08 mg/kg). Fur was shaved, and the area was prepared with isopropanol and betadine. Pellets were implanted subcutaneously at the base of the neck using a trochar and the incision sealed with cyanoacrylate tissue glue. Mice were observed daily for three days following the procedure and then 3-4 times per week. One mouse (prednisolone + AAV8-Ostn group) was euthanized early due to wound dehiscence and removed from the study. Four weeks after pellet implantation, mice were euthanized with CO_2 followed by cervical dislocation, and tissues were collected for analysis. All procedures involving animals were performed in accordance with guidelines issued by the Institutional Animal Care and Use Committees (IACUC) in the Center for Comparative Medicine at the Massachusetts General Hospital and Harvard Medical School under approved Animal Use Protocols (2019N000201). All animals were housed in the Center for Comparative Medicine at the Massachusetts General Hospital (21.9 $\pm$ 0.8°C, 45 $\pm$ 15% humidity, and 12-h light cycle 7 am–7 pm). Final animal numbers in each group were as follows: AAV8+Control & Placebo: n = 10; AAV8-Control & Prednisolone: n = 8; AAV8+Ostn & Placebo: n = 8; AAV8-Ostn & Prednisolone: n = 8.

METHOD DETAILS

Serum

Just prior to euthanasia, whole blood was collected via cheek bleed into serum separator tubes (BD). Blood was allowed to clot for at least 10 min, then centrifuged for 10 min at 4°C to separate the serum. Serum was stored at −80°C until analysis by procollagen type 1 N-terminal peptide (P1NP) and C-terminal collagen crosslinks (CTX) assays (IDS) based on the manufacturer's instructions.

RNA

Liver and bone were collected for RNA immediately following euthanasia. A portion of the liver was flash-frozen in liquid nitrogen and stored at −80°C. Liver tissue was pulverized in TRIzol and RNA isolated using chloroform followed by precipitation in isopropanol. Humeri were dissected and cleaned of muscle. The epiphyses were trimmed, bones were transferred into microcentrifuge tubes, and marrow was removed by centrifugation (17,000G for 15 s at RT). Bones were then snap-frozen in liquid nitrogen and stored in liquid nitrogen. Bones were pulverized in TRIzol and RNA extracted using chloroform followed by precipitation in isopropanol and column purification (PureLink RNA Mini Kit, Invitrogen). Two humeri (placebo + AAV8-control and prednisolone + AAV8-control) were mislabeled and excluded from further analysis. RNA was DNase treated and reverse transcribed to cDNA (PrimeScript, Takara) before SYBR green-based RT-qPCR on an Applied Biosystems StepOnePlus system (Table S1).

Micro-CT

One femur and the fifth lumbar (L5) vertebra from each animal were dissected and stored in cold 70% ethanol until scanning. Micro-CT imaging was performed on a bench-top scanner (μCT40, Scanco Medical AG, Brüttisellen, Switzerland) to measure the morphology of the femoral mid-diaphysis, femoral distal metaphysis, and L5 vertebral body. For the femoral cortical bone, a 500 μm region of the mid-diaphysis was scanned using 70 kVp peak X-ray tube potential, 113 mA X-ray tube current, 200 ms integration time, and 10 μm isotropic voxels. Cortical bone was segmented from soft tissue with a threshold of 700 mg HA/cm^3. For the femoral trabecular bone, a 1500 μm region of the mid-diaphysis, starting 1700 μm proximal to the distal growth place and extending distally, was scanned using the same settings. For the L5 vertebral trabecular bone, a 1500 μm region was scanned using the same settings. Upon scanning, three of the vertebral samples were discovered to be sacral rather than lumbar and were excluded

from analysis (one placebo + AAV8-Ostn, one prednisolone + AAV8-control, and one prednisolone + AAV8-Ostn). Cancellous bone was segmented from soft tissue using a threshold of 300 mg HA/cm^3 and separated from cortical bone with a semiautomated contouring program. Scanning and analysis was performed in the Scanco Evaluation Program in a blinded manner and adhered to the guidelines for the use of micro-CT for the assessment of bone architecture in rodents (Bouxsein et al., 2010).

Flexural testing

One femur from each animal was dissected and stored in PBS-wrapped gauze at −20°C. Two bones were broken (placebo + AAV8-Ostn) or lost (prednisolone + AAV8-Ostn) and therefore excluded from analysis. Prior to mechanical testing, the femurs were micro-CT scanned at the mid-diaphysis while submerged in PBS in order to calculate moment of inertia. Femurs were mechanically tested in three-point bending using an electrical force materials testing machine at room temperature (Electroforce 3230, Bose Corporation, Eden Prairie, MN). The bending fixture had a bottom span length of 8 mm (approximately 50% bone length). Bones were positioned with the cranial surface resting on the supports and being loaded in tension. The test was performed in displacement control at 0.1 mm/s with force and displacement data collected at 50 Hz. Bending rigidity was calculated using the linear portion of the force-displacement curve. Yield was determined when the secant slope of the force-displacement curve was reduced by 10%. The minimum moment of inertia (Imin) measured with micro-CT was used when calculating modulus and stress. Work to yield and work to fracture are the energy that was required to cause the femur to yield or fracture, respectively, and they were calculated by finding the area under the force-displacement curve using the Riemann Sum method.

Histology

Tibias were dissected and fixed in 10% neutral-buffered formalin for 24 h. Bones were decalcified in EDTA for two weeks, then one bone was dehydrated in graded ethanols and embedded in paraffin. The contralateral tibia was incubated in 30% sucrose solution and embedded in OCT compound. 5 μm longitudinal sections were obtained from paraffin blocks and 10 μm longitudinal sections were obtained from frozen blocks.

Frozen sections were washed in PBS, post-fixed in 4% paraformaldehyde (PFA), permeabilized in 0.05% saponin, and stained with phalloidin for 30 min (1:1000, Abcam). After washing, samples were incubated with DAPI (Invitrogen, 5 μg/mL) for 15 min, washed again, and coverslips mounted with Fluoromount-G. Imaging was conducted on a Zeiss Airyscan confocal microscope with a 40x oil-immersion objective.

Paraffin sections were deparaffinized in three changes of xylene and hydrated through graded ethanols, then used for hematoxylin & eosin (H&E), terminal deoxynucleotidyl transferase dUTP nick end labeling (TUNEL), RNAscope, silver nitrate, and tartrate-resistant acid phosphatase (TRAP) assays. H&E staining was performed using standard protocols, followed by imaging on a Keyence BZ-X710 microscope at 20x.

For TUNEL, rehydrated sections were post-fixed in 4% PFA and permeabilized with PCR-grade Proteinase K (20 μg/mL) for 30 min at 37°C. Samples were incubated with TUNEL reaction mixture (Roche) for 60 min at 37°C followed by DAPI, then mounted with Fluoromount-G. Fluorescent images were captured at 20x on a Nikon Eclipse Ni microscope.

RNA *in situ* hybridization for Ostn was performed with RNAscope 2.5 HD Assay-Brown (Advanced Cell Diagnostics). Tibia sections were prepared by deparaffinization in fresh xylene and 100% ethanol, then dried in a 60°C oven for 30 min. Samples were incubated with hydrogen peroxide at room temperature for 10 min, then with pepsin for 30 min at 40°C. After washing, samples were incubated with target probe (Ostn, NM_198112.2, region 2-1144) and amplified following the manufacturer's instructions. Signal was detected using DAB for 10 min, then sections were briefly counterstained with 50% hematoxylin, dehydrated, cleared, and mounted. Brightfield images were captured at 20x on a Nikon Eclipse Ni microscope.

Silver nitrate staining solution was freshly prepared from two parts 50% silver nitrate and one part 2% gelatin type A with 1% formic acid (Fowler et al., 2017). Sections were incubated for 55 min in the dark, then washed and incubated in 5% sodium thiosulfate for 10 min. After dehydrating and mounting, images were captured on a Keyence microscope system at 40x.

For TRAP staining, sections were rehydrated to water, then incubated in 0.2 M acetate buffer (pH 5.0) for 30 min. TRAP staining solution was freshly prepared with 0.5 mg/mL Napthol As-MX Phosphate and

1.1 mg/mL Fast Red TR salt in 0.2 M acetate buffer, and samples were incubated for 30 min at 60°C. Slides were then rinsed in water, counterstained in Fast Green for 1 min, dipped in 1% acetic acid, rinsed in water, and mounted with aqueous medium. Imaging was conducted on a Nanozoomer slide scanner (Hamamatsu).

Image quantification

All analyses were performed on a blinded basis using images from uniform areas from at least four regions of interest (ROIs) representing the anterior and posterior cortex of the tibia. The number of osteocyte nuclei and empty lacunae was counted in four H&E stained images per bone to calculate the proportion of empty lacunae. For TUNEL and TRAP staining, the proportion of positively-stained osteocytes was calculated relative to total DAPI-stained nuclei and total cortical bone area, respectively.

In silver nitrate-stained bones, the length of ten dendrites on each of three osteocytes in all four ROIs was measured using ImageJ (120 dendrites/mouse). Additionally, the total number of dendrites was counted for five representative osteocytes in all four ROIs. For phalloidin-stained bones, signal from osteocyte cell bodies was removed using DAPI as a mask, and images were uniformly thresholded to remove background. The density of osteocyte dendrites was calculated as the percent of image area stained by phalloidin.

Flow cytometry

Ocy454 cells treated with CNP, Ostn, or dexamethasone were resuspended in cold FACS buffer and incubated at 4°C with gentle rocking for 30 min. Approximately 100,000 cells per replicate were incubated with 0.2 μg PE-conjugated anti-cd61 antibody or isotype control (Invitrogen) in 100 μL FACS buffer for 45 min at 4°C in the dark. Cells were washed twice in FACS buffer, then resuspended in Annexin Binding Buffer with Annexin V conjugate for 15 min at room temperature in the dark. Flow cytometry was performed on an Attune NxT (Thermo Fisher Scientific), with dead cells, debris, and doublets excluded by FSC, SSC, and Annexin V gating. Flow cytometry data were analyzed using FlowJo (version 10) to calculate median fluorescence intensity of live, single cells in each replicate.

QUANTIFICATION AND STATISTICAL ANALYSIS

For analysis of *in vivo* gene expression data (2 groups), groups were compared using unpaired 2-tailed t-tests. For *in vitro* gene expression data (3 groups), analysis was performed using 1-way ANOVA followed by pairwise comparisons of groups with Tukey's multiple comparisons tests. To analyze the effects of prednisolone and osteocrin on bone, two-way ANOVA was performed, followed by Sidak's multiple comparisons tests between placebo- and prednisolone-treated mice within the same AAV8 treatment group. The ROUT method (Q = 1%) was used to remove outliers from each analysis (GraphPad Prism 8.4), as indicated in figure legends. p values less than 0.05 were considered to be significant. Animal numbers in each group were as follows: AAV8+Control & Placebo: n = 10; AAV8-Control & Prednisolone: n = 8; AAV8+Ostn & Placebo: n = 8; AAV8-Ostn & Prednisolone: n = 8, with any excluded samples noted in figure legends. Each plotted data point represents one independent biological replicate.